State-selective quantum interference observed in the photorecombination of $Hg^{75+...78+}$ ions at the Heidelberg EBIT

A. J. González Martínez, J. R. Crespo López-Urrutia, * and J. Ullrich
Max-Planck Institute for Nuclear Physics, Saupfercheckweg 1, D-69117 Heidelberg, Germany

Abstract

The well-known Fano-profiles appearing in differential photonionization cross sections when resonances are present can also be observed in the time-reversed process of photorecombination of highly charged ions, where direct and indirect processes leading to the same final quantum state of the ion and the photon field can interfere, thus producing asymmetric lines shapes. Experiments performed at the Heidelberg electron beam ion trap with $Hg^{75+...78+}$ ions have delivered state-selective Fano parameters and accurate resonance energies.

Key words:
Photorecombination, dielectronic recombination, radiative recombination, highly charged ions, quantum interference
PACS: 34.80.Kw, 32.80.Hd, 52.25.Os

1. Introduction

The classic work of Fano [1,2] exposed the effects of quantum interference in the inelastic scattering of electrons from He-atoms. He observed line asymmetries caused by quantum interference in the electron energy-loss spectra. These so-called Fano profiles were later also found in the photoionization process, and are rather general phenomena. Remarkable features present in the energy-dependent cross section and strong contributions to the total photoionization cross sections could be explained by taking them into account. High-resolution synchrotron experiments using atoms or molecules in the gas phase need to include such effects in the data analysis, since otherwise the asymmetry of the resonances could *e. g.* result in a systematic error in the determination of the corresponding energies. In many other fields of physics, quantum interference also produces subtle but measurable effects.

While the photoionization of atoms and molecules has been studied intensively by means of synchrotron radiation by many groups, photoionization experiments with ions are still technically challenging, due to the low density of the ion beams used as targets. Ions in low charge states, such as Ti^{2+} and Sc^{2+}, have been investigated recently in great detail *e. g.* at the Advanced Light Source in Berkeley [3,4]. Highly charged ions (HCI) have never been studied with synchrotron radiation, as their difficult production results in correspondingly extremely low target densities.

* Max-Planck Institute for Nuclear Physics, Saupfercheckweg 1, D-69117 Heidelberg, Germany
Email address: crespojr@mpi-hd.mpg.de (J. R. Crespo López-Urrutia,).

Nonetheless, with the advances in the ion source and accelerator technology, it has become in principle possible to study experimentally the time-reversed processes, namely photorecombination, to test the same physical mechanisms (see Fig. 1).

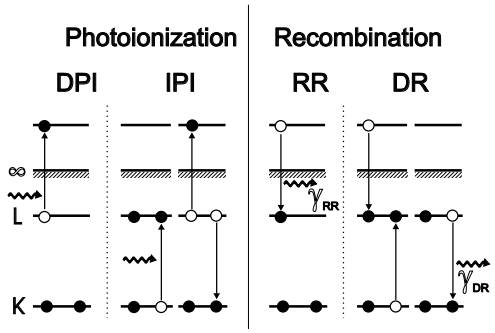

Fig. 1. (left) Two different photoionization channels: direct (DPI) and indirect photoionization (IPI). (right) The corresponding time reversed processes in the photorecombination are the radiative (RR) and dielectronic (DR) recombination.

The photorecombination of low-charge state ions has been experimentally accessible at storage rings (see, *e. g.*, the work by Schippers *et. al.* [5]). As an example of recent work carried out with HCI, Brandau *et. al.* [6,7] have used the ESR storage ring, filled with stochastically cooled ion beams, to study the deep inner-shell resonances of H-like U^{91+} ions. The lack of a photon detection system in most of these experiments still somewhat limits their scientific potential. A useful review of these research can be found in [8]. Experiments using electron beam ion sources (EBIS) and traps (EBIT) also yielded a wealth of data on the photorecombination of HCI, starting with the pioneering work of Ali [9] and Knapp [10].

In both storage rings and EBITs, ions up to the highest charges states, such as U^{92+}, have been investigated, and total and differential cross sections have been obtained. EBITs are ideal devices for the study of HCI photorecombination for the following reasons: a) the charge state of the trapped HCI can be chosen, and the charge state distribution can be concentrated in one or a few charge states; b) a high density, but nearly monoenergetic electron beam is available in the trap region, providing the needed electrons; and c) energy-resolving photon detectors can be placed with appropriate solid angles in close proximity to the reaction region. With these ingredients, experiments equivalent to photoionizing HCI by means of hard x-rays can be performed with a relatively compact experimental setup. The Heidelberg EBIT [11] (see Fig. 2) has a dedicated setup for the study of photorecombination, which has already been used *e. g.* to study the effect of the two-electron-one-photon transition in the dielectronic resonances of He-like Ar^{16+} [12] or the dielectronic resonances of Ge^{30+} [13]. This apparatus has recently been improved for precision experiments at higher energies.

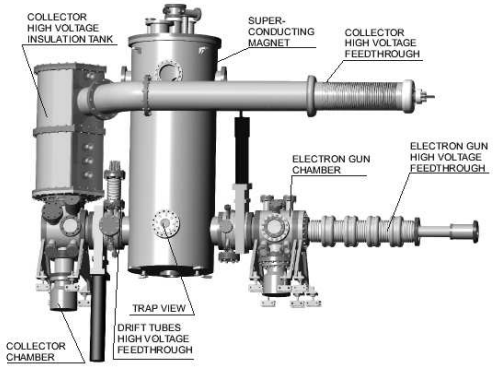

Fig. 2. Artist's view of the Heidelberg EBIT.

Under normal circumstances, one can treat the photorecombination to a good approximation as the sum of the direct process (the so-called radiative recombination, RR) and the strongest indirect process, dielectronic recombination (DR, which can be viewed as the time-reversed Auger effect), and, for low-Z ions, ignore quantum interference effects between DR and RR. For highly charged ions (HCI) however, strong interference effects are expected, since the RR transition matrix element scales with Z, and hence becomes for high Z values comparable in magnitude to the DR matrix element, which is roughly independent of Z. Due to these facts, the RR cross section scales with Z^2, while the DR cross sections remain more or less the same. The amplitudes of the two indistinguishable quantum paths to recombination become similar, and interference effects become noticeable (see Fig. 3). Despite of this, the observation of such an effect remained elusive for a long time. This was a consequence of the problematic preparation of

the initial states of the reaction partners, ions and electrons, and also of difficulties in the determination of the final quantum state of the system, where a recombined ion and a photon appear.

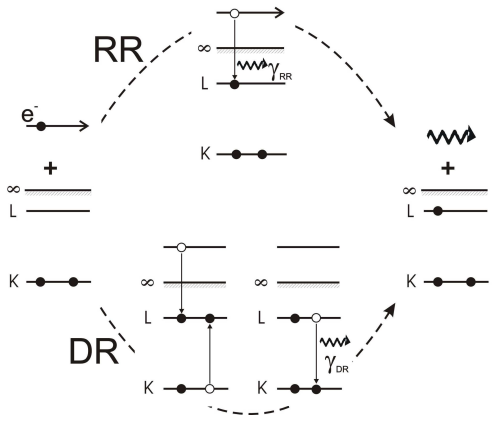

Fig. 3. In the photorecombination process, the quantum state of the total system can evolve from its initial state (monoenergetic electron, ion in ground state) to its final state (recombined ion, monoenergetic photon) through two different paths, resulting in quantum interference.

The first observation of Fano profiles resulting from this quantum interference in photorecombination processes was reported by Knapp *et. al.* [14] in 1995. In that experiment, the KLL resonances of photorecombining uranium ions in very high charge states displayed clear asymmetries which were interpreted as the signature of quantum interference. However, it was not possible at that time to separate the contributions from different electronic states to the total process. In a recent experiment at the Heidelberg EBIT by González Martínez *et.al.* [15], improved resolution of the photon exit channel, enhanced statistics, and careful analysis have allowed for the first time the observation of this phenomenon with state selectivity, and to determine the Fano profiles of individual resonances with error bars of only 6%.

Another important aspect of these measurements is the fact that, for heavy HCI, QED contributions are very large, namely of the order of 200 eV, as illustrated in Table 1, and thus these results are sensitive *e. g.* to the self-energy (SE) and vacuum polarization (VP) with screening contributions. This is one of the main motivations of this work: the test of calculations of QED contribution caused by the very strong electromagnetic fields present in HCI. Few-electron ions are most convenient for these purposes, as the electron correlation effects become less pronounced. However, the electronic structure of high–Z heavy ions is also strongly affected by nuclear size effects. In the present case, they cause a shift of the 1s state of approximately 50 eV. This situation could seem not very well suited for the study of any of these two phenomena, given their intertwinning. Nonetheless, both QED and nuclear size effects do not have the same dependency on the nuclear charge Z, and they couple with various degrees of strength to the different electronic configurations. Therefore, it is possible to disentangle their contributions if, for instance, several charge states and/or electronic configurations are investigated with high precision. For these reasons it is also important to study isoelectronic sequences, thereby gaining additional information about the systematics of these dependencies.

Table 1
Theoretical QED contributions (in eV) to the $1s^2$ and $1s2s^2$ states for $Hg^{78+...77+}$ ions (from [16]).

Contribution	$1s^2$	$1s2s^2$
one-electron VP	- 90.2	-59.6
VP with screening	-88.9	-58.3
one-electron SE	414.5	278.4
SE with screening	408.9	275.0
one-electron QED=VP+SE	324.3	218.8
QED=VP+SE with screening	320.0	216.7

2. Experiment

The principle of an electron beam ion trap is explained in Fig. 4. An electron beam of 160 mA was accelerated by a variable potential of up to 68 kV and compressed to a diameter of roughly 0.05 mm by means of an axial 8 T magnetic field generated by a superconducting magnet. In the negative space charge of this beam, positive ions were radially confined and succesively brought to

higher charge states (here up to Hg^{78+}) through collisions with the beam electrons. The final charge state limit is reached when the electron energy is not sufficient to overcome the ionization potential of the remaining electrons. A central ring-shaped

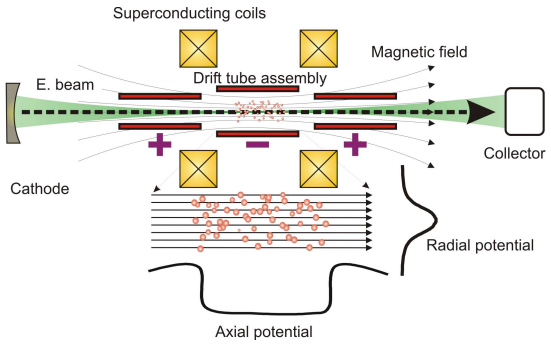

Fig. 4. Principle of an electron beam ion trap.

electrode, biased at a negative potential in relation to its neighbouring electrodes, was used to create a longitudinal potential well, thus producing a three dimensional trap. In this way, a cloud containing 10^5–10^7 trapped ions in a 40 mm length and roughly 0.2 mm diameter volume was stored in the central drift electrode. Not only ionization by electron impact, but also electron-ion photorecombination takes place at high rates within this volume due to the strong overlap of the electron beam (with a density of up to 10^{13} e/cm^3) and the ion cloud (up to 10^{10} ions/cm^{-3}). The trap region inside the central drift tube can be observed with different detectors and spectrometers.

A variable photon energy in the photoionization process corresponds to a variable electron energy in the time-reversed photorecombination experiment. The x-ray photons emitted by the recombining ions while scanning the electron beam energy slowly were monitored by means of a Ge-detector mounted at 90° relative to the electron beam axis, which registered the photons' energies. The electron energy was ramped up und down very slowly (40 V/s) in order to maintain equilibrium between the photorecombination process and electron impact ionization, which continuously replenishes the losses in the ion population of the recombining charge states. The electron beam energy was determined from a measurement of the acceleration

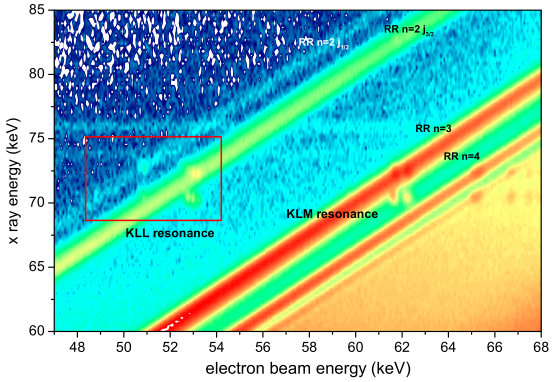

Fig. 5. Plot of the hoton yield measured in the photorecombination of $Hg^{75+..78+}$ ions with electrons of energies from 47 keV to 68 keV. Diagonal bands due to radiative recombination into unocuppied (or open) shells with principal quantum numbers n and features resulting from DR resonances can be seen here. The region enclosed inside the red rectangle was investigated in more detail (see Fig.6)

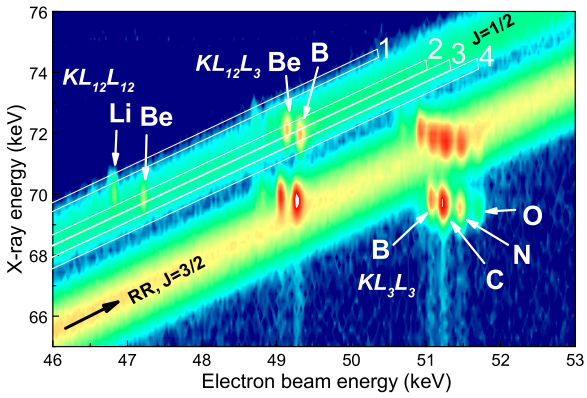

Fig. 6. Logarithmic contour plot of the $Hg^{75+..78+}$ ions' KLL resonances. The upper diagonal band results from RR into $n = 2, J = 1/2$ and the lower from $n = 2, J = 3/2$ (bottom) states. DR resonances appear superimposed as bright spots. The areas enclosed labelled 1,...,4 in the upper RR band mark regions whose projection onto the electron beam axis is shown in Figs. 7 and 8.

potential applied to the cathode and drift tubes, corrected for space charge contributions due to the electron beam charge density and its compensation by the trapped ions. The acceleration potential was measured by means of a high-accuracy voltage divider. The arrival of an x-ray photon (γ_{DR}, γ_{RR}, or bremsstrahlung) triggered each single event acquisition process. Photon and electron beam energies were simultaneously recorded and stored event by

event. In this way, two-dimensional maps (photon vs. electron energy) were accumulated. The first one, displayed in Fig. 5) gives a general overview, with beam energies ranging from 47 keV to 68 keV. A more detailed map was obtained by varying the beam energy across the region were the $Hg^{75+..78+}$ ions' KLL resonances (45-53 keV) (see Fig. 6) appear.

The plots shows clearly visible diagonal bands, which are due to RR into levels with different principal quantum number n. The photon energy in this process corresponds to the sum of the captured electron's kinetic energy plus the binding energy of the final electronic state. Thus, the photon energy increases linearly with the lectron energy. In Fig. 6, the upper band represents RR into states $n = 2$ with the total angular momentum $J = 1/2$, and the lower, broader band into those with $J = 3/2$. The x-ray energy difference between the two bands is approximately 2 keV. A higher yield of x-rays appears concentrated on five clusters of horizontally aligned bright spots, due to several strong DR resonances. Following the customary nomenclature [14], these resonances are labelled $KL_{12}L_{12}$ (left one), $KL_{12}L_3$ (two central clusters) and KL_3L_3 (two right clusters). Four of the clusters strongly overlap with the RR bands. For a He-like ion in an initial state $1s^2$, DR processes result into population of the final states $KL_{J=1/2}L_{J=1/2}$ ($1s2s^2$, $1s2s2p_{1/2}$, $1s2p_{1/2}2p_{1/2}$), $KL_{J=1/2}L_{J=3/2}$ ($1s2s2p_{3/2}$, $1s2p_{1/2}2p_{3/2}$) and $KL_{J=3/2}L_{J=3/2}$ ($1s2p_{3/2}2p_{3/2}$), respectively. These denominations are also used analogously for other charge states.

By projecting specific regions of this plot either onto the electron beam or onto the x-ray energy axis (see Figs. 7,8,9), that is, by slicing the broad diagonal bands into narrow cuts, the interference for specific charge states can be studied separatedly, because the photon energies on the different slices of each RR band correspond to different ion charge states. For example, the top slice of the RR $J = 1/2$ band shows the He-like ion charge state along with a fraction of Li-like ions (Fig. 7a, cut 1). In contrast, in the next lower slice, a strong Be-like peak is observed with only a very weak contribution from a Li-like resonance (Fig. 7b, cut 2). The lowest slice of this band showed almost an exclusive population of B-like ions Fig. 8, cut 4). Other cuts parallel to the $J = 3/2$ band but shifted to lower x-ray energies pass through a set of DR resonances which do not overlap with the RR process, as the photon was emitted by a transition from a $J = 1/2$ level whereas the foregoing recombination took place into a $J = 3/2$ vacancy. Therefore, these photons have an energy different from those produced by RR at the same electron beam energy. Thus, no quantum interference can occur here, and accordingly the observed line profiles were symmetrical (see Fig. 9).

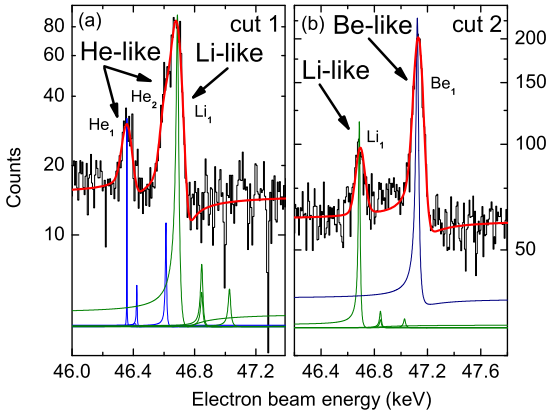

Fig. 7. Experimental (black curve) and fitted (red curve) data for two different slices of the RR into $n = 2, J = 1/2$ in the $KL_{12}L_{12}$ region whose analysis shows negative Fano factors in comparison with a normalized non-convoluted theoretical cross section (blue and green curves). Left: Projection of the upper slice where He-like and Li-like ions are observed. Right: Projection of an intermediate region showing Be- and Li-like resonances.

Since the resonances showed asymmetric profiles, Fano profiles had to be used in order to determine their excitation energies. The Fano parameter of each resonance was left free during the iterations. It was convoluted in each case with a normalized Gaussian distribution to account for the electron beam energy spread of about 60 eV at 50 keV electron beam energy E_e, corresponding to a relative resolution $\Delta E_e/E_e \approx 1/1000$. Due to this good resolution, the Fano factors can be determined for well-resolved individual resonances (see Table 2). For the fitting procedure, the natural width Γ_d of each DR resonance is the only parameter taken from theory. The fit quality was evaluated with the χ^2 over degrees-of-freedom (DoF) method. In fact,

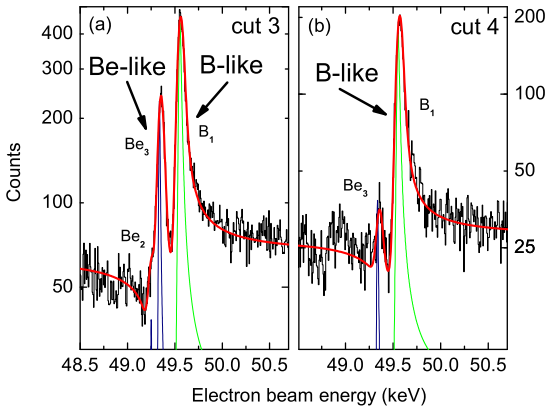

Fig. 8. $KL_{12}L_3$ Be- and B-like resonances showing Fano factors opposite (*i. e.*, positive)to those of the He- and Li–like resonances (negative) in the $KL_{12}L_{12}$ region (see Fig. 7). The two cuts exemplify how to resolve resonances from specific charge states. Also displayed are the normalized non-convoluted theoretical cross sections (blue and green curves).

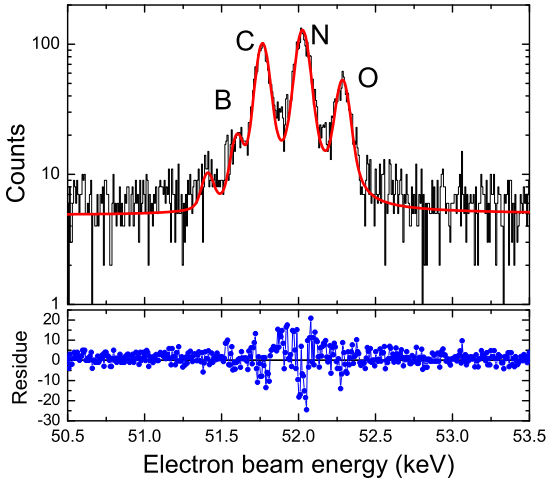

Fig. 9. Projection of non-interfering photon deexcitation channels for the $J = 3/2$ DR resonances of the B- to O-like mercury ions showing symmetric line profiles.

Table 2
Theoretical (MCDF) and measured Fano factors (q), and measured energies of some DR resonances. The He-like $(1s2s^2)_{1/2}$ resonance was used as energy reference

	Excited state	J	q_{theo}	q_{meas}	E_e(keV)
Li_1	$1s2s^22p_{1/2}$	1	-12.2	-14.2(2.2)	46.686(5)
Be_1	$1s2s^2(2p_{1/2})^2$	1/2	-12.0	-9.3(0.9)	47.135(5)
Be_3	$(1s2s^22p_{1/2})_02p_{3/2}$	3/2	7.3	6.7(0.6)	49.349(6)
B_1	$1s2s^2(2p_{1/2})^22p_{3/2}$	1	5.2	5.1(0.3)	49.557(4)
B_2	$1s2s^2(2p_{1/2})^22p_{3/2}$	2	9.0	10.0(1.0)	49.499(4)

the Fano fits yielded a much better χ^2/DoF than Lorentzian fits.

Another relevant check was to analyze the cuts between RR into $n = 2, J = 3/2$ and RR into $n = 3$, where the states populated by the DR process decay to the ground state via two cascading transitions, and interference cannot happen (Fig. 9). Such projections resulted in very high values of the Fano parameter, *i. e.*, the line profiles were symmetric, as expected.

In Table 2, the experimentally determined scale (which was accurate to a level of ± 14 eV) was not used, but we have referenced the energy scale to the theoretical value (obtained by the MCDF method, see [15]) of the He-like $(1s2s^2)_{1/2}$ resonance, since it results in a shift of only approximately 5 eV at 50 keV in comparison with the value obtained by the experimental calibration. Given the excellent agreement of different predictions with respect to this and other He-like resonances, its value seems to be very suitable as energy reference.

The atomic structure calculations for He-like ions are expected to be the most reliable among those for many-electron systems. Indeed, they show the smallest deviations from the experimental results, typically a few eV, as one can see in Fig.10. Therefore, using this single theoretical reference, a relative energy scale spanning more than 5 keV (at ≈ 50 keV), and valid for all ionization stages from He- to O-like was established; more details will be given in a forthcoming paper [17].

In conclusion, the high resolution studies of the dielectronic resonances in very heavy HCI can yield important information on the electronic structure. The data shown here have provided some rigorous tests of different theoretical models at the level of a few electron volts. Since the excitation energies investigated include large QED and relativistic corrections, the present method seems competitive in comparison with other state-of-the-art spectroscopic techniques, such as the transmission crystal spectrometer FOCAL [18] and the use of decceleratedions at the ESR [19]. Further improvements and a more accurate calibration of the experiment

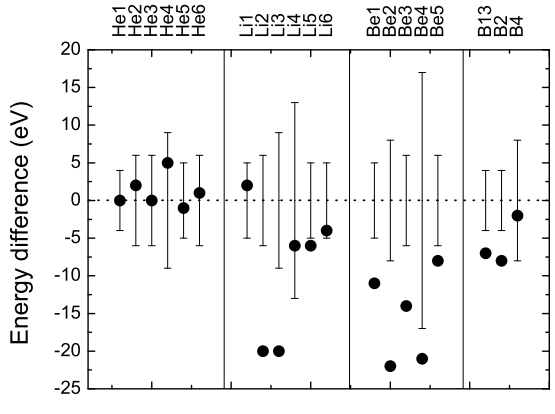

Fig. 10. Difference (in eV) between experimental and theoretical (MCDF, this work) results for the measured DR resonance energies of the He- to B-like mercury ions. The experimental energies were adjusted to the theoretical value of the $(1s2s^2)_{1/2}$ state energy. The error bars shown are those of the experiment.

should, in principle, allow us in the near future to approach an accuracy of 1 eV, or the order of 10 ppm.

References

[1] U. Fano, Phys. Rev. **124**, 1866 (1961).

[2] U. Fano and J. W. Cooper, Phys. Rev. **137**, A1364 (1965).

[3] S. Schippers, A. Müller, S. Ricz, M. E. Bannister, G. H. Dunn, J. Bozek, A. S. Schlachter, G. Hinojosa, C. Cisneros, A. Aguilar, A. M. Covington, M. F. Gharaibeh, and R. A. Phaneuf, Phys. Rev. Lett **89**, 193002 (2002).

[4] S. Schippers, A. Müller, S. Ricz, M. E. Bannister, G. H. Dunn, A. S. Schlachter, G. Hinojosa, C. Cisneros, A. Aguilar, A. M. Covington, M. F. Gharaibeh, and R. A. Phaneuf, Phys. Rev. A **67** 032702(2003).

[5] S. Schippers, S. Kieslich, A. Müller, G. Gwinner, M. Schnell, A. Wolf, A. Covington, M. E. Bannister, and L.-B. Zhao, Phys. Rev. A **65**, 042723 (2002).

[6] C. Brandau *et al.*, in *XXIII ICPEAC, Stockholm, Sweden, 2003, Abstracts of Contributed Papers*,(2003) p. Fr091.; also in *GSI Scientific Report 2002*, p. 91-92.

[7] C. Brandau, C. Kozhuharov, K. Beckert, P. Beller, D. Bernhardt, F. Bosch, S. Bhm, F.J.Currell, B. Franzke, A. Gumberidze, Z. Harman, J. Jacobi, P.H. Mokler, F. Nolden, A. Müller, W. Scheid, S. Schippers, E. Schmidt, U. Spillmann, Z. Stachura, M. Steck, and Th. Stöhlker *GSI Scientific Report 2004*, p. 201 (Gesellschaft für Schwerionenforschung, Darmstadt, 2005)

[8] H. F. Beyer and V. P. Shevelko (eds.), *Atomic Physics with Heavy Ions*, (Springer, Heidelberg, 2002).

[9] R. Ali, C. P. Bhalla, C. L. Cocke, and M. Stöckli,Phys. Rev. Lett. **64** 633 (1990).

[10] D. A. Knapp, R. E. Marrs, M. A. Levine, C. L. Bennet, M. H. Chen, J. R. Henderson, M. B. Schneider, and J. H. Scofield, Phys. Rev. Lett. **62** 2104 (1989).

[11] J. R. Crespo López-Urrutia, A. Dorn, R. Moshammer, and J. Ullrich, Phys. Scr. **T80**, 502 (1999).

[12] Y. Zou, J. R. Crespo López-Urrutia, and J. Ullrich, Phys. Rev. A **67**, 42703(2003).

[13] X. Zhang, J. R. Crespo López-Urrutia, P. Guo, V. Mironov, X. Shi, A. J. González Martínez, H. Tawara and J. Ullrich, Journal of Physics B: Atomic, Molecular and Optical Physics **37**, 2277 (2004).

[14] D. A. Knapp, P. Beiersdorfer, M. H. Chen, J. H. Scofield, and D. Schneider, Phys. Rev. Lett. **74**, 54 (1995).

[15] A. J. González Martínez, J. R. Crespo López-Urrutia, J. Braun, G. Brenner, H. Bruhns, A. Lapierre, V. Mironov, R. Soria Orts, H. Tawara, M. Trinczek, and J. Ullrich, Phys. Rev. Lett. **94**, 203201 (2005)

[16] Z. Harman, priv. comm.

[17] A. J. González Martínez, to be submitted to Phys. Rev. A.

[18] H. F. Beyer *et. al.*, *GSI Scientific Report 2004*, p. 215 (Gesellschaft für Schwerionenforschung, Darmstadt, 2005)

[19] A. Gumberidze, Th. Stöhlker, D. Bana, K. Beckert, P. Beller, H. F. Beyer, F. Bosch, S. Hagmann, C. Kozhuharov, D. Liesen, F. Nolden, X. Ma, P. H. Mokler, M. Steck, D. Sierpowski, and S. Tashenov, Phys. Rev. Lett. **94**, 223001 (2005).